Nonlinear Dynamics **13:** 243–257, 1997.

Hydrodynamic and Geometric Stiffening Effects on the Out-of-Plane Waves of Submerged Cables

M. BEHBAHANI-NEJAD and N. C. PERKINS
Mechanical Engineering and Applied Mechanics, The University of Michigan, Ann Arbor, MI 48109, U.S.A.

(Received: 9 April 1996; accepted: 3 February 1997)

Abstract. This study focuses on the relative importance of two sources of nonlinearities affecting submerged cable response. The first of these is the added fluid damping offered by the surrounding medium while the second is the geometric stiffening offered by the cable through finite extensions of its centerline. The contribution of each nonlinear effect, taken separately and in tandem, is evaluated herein through the study of structural waves that form in the (out-of-plane) direction normal to the cable equilibrium plane.

Numerical solutions are pursued herein using a finite difference algorithm which is brought to bear on two nonlinear cable/fluid models including: (1) a nonlinear submerged cable model in which hydrodynamic drag is the sole nonlinear mechanism (referred to herein as the *nonlinear drag model*); and (2) a nonlinear submerged cable model in which hydrodynamic drag and geometric stiffening are both active nonlinear mechanisms (the *nonlinear elastic-drag model*). Numerical solutions for propagating cable waves are developed for the case of a long suspension subjected to a concentrated harmonic excitation source. Conclusions are subsequently drawn regarding the spatial decay of the resulting out-of-plane waves and the dynamic cable tension induced by these waves. The effect of these two nonlinear mechanisms is further explored through the analysis of two additional, linear models: (3) a simple linear taut string model without drag (the *simple model*); and (4) a linear taut string model with linear drag (the *linear drag model*). The results of all models are critically compared and the range of validity of the linear/cable fluid models are assessed.

Key words: Wave propagation, submerged cable, structural dynamics, fluid/structure interaction.

1. Introduction

This investigation addresses the need to understand the dynamics of submerged cables employed in ocean engineering applications including: towing and mooring systems, oceanographic and ranging systems, and tether and umbilical systems. In all of these applications, the submerged cable is excited by loads that originate from the surrounding fluid environment (e.g., currents and waves) and from the motion of attached bodies (e.g., motions of instruments, buoys, vessels). The ensuing cables motions may significantly influence the performance of the cable and the mission that it is designed to support. Thus, accurate predictions of dynamic response are often desired to design or to evaluate cable/system performance.

Predictions of dynamic cable response may, at times, follow from low-order cable models assuming the participation of a few selected cable modes. While computationally simple, this modal approach becomes less feasible for very long cable suspensions or for higher frequency/shorter wavelength dynamics due to high modal density. In such instances, an attractive alternative is to describe the cable response in terms of propagating waves, in lieu of standing waves (cable modes) [2, 4]. To this end, this study contributes a fundamental understanding of nonlinear wave propagation along a fluid-loaded cable, specifically for the case of out-of-plane structural waves.

This study focuses on the relative importance of two sources of nonlinearities affecting submerged cable response. The first of these is the added fluid damping offered by the

surrounding medium while the second is the geometric stiffening offered by the cable through finite extensions of its centerline. The contribution of each nonlinear effect, taken separately and in tandem, is evaluated herein through the study of structural waves that form in the out-of-plane direction. While these waves may, in general, also induce in-plane cable response, the present study focuses exclusively on the simpler out-of-plane response. Taken with the recently developed *linear* theory governing the in-plane structural waves [2, 4], the present investigation on nonlinear cable waves provides a further step towards a complete nonlinear, three-dimensional theory.

The study of cable structural waves is related to the theory of wave propagation of a simple string which is a classical subject treated in numerous sources [5–10]. The addition of lumped masses (instruments) alters the characteristics of free wave propagation on strings as evaluated by Lili and Vandiver using the transfer matrix method [11]. Few studies, however, have considered either nonlinear waves resulting from either geometrically large motions and/or fluid/structure interaction.

Chapman [13] numerically simulated the effects of deterministic and random ship disturbances that propagate through a submerged, sagged string or "cable" to a neutrally buoyant towed-fish. Motivated by similar applications, Dowling [14] investigated the dynamic response of a towed flexible cylinder and a faired cable using analytical methods. Focusing on the propagation of a disturbance along the faired cable to the cylinder due to unsteady ship motion, Dowling concluded that cable wave propagation depends strongly on the ship velocity, the frequency of the disturbance, and the cable length. Dowling's studies further concentrate on the singularity in the cylinder or cable where cylinder or cable tension equals the hydrodynamic forces.

The nonlinearities due to hydrodynamic drag and geometric stiffening render the cable/fluid model intractable by exact analytical methods. Numerical solutions are pursued herein using a finite difference algorithm. This algorithm is brought to bear on two nonlinear cable/fluid models including: (1) a nonlinear submerged cable model in which hydrodynamic drag is the sole nonlinear mechanism (referred to herein as the *nonlinear drag model*); and (2) a nonlinear submerged cable model in which hydrodynamic drag and geometric stiffening are both active nonlinear mechanisms (the *nonlinear elastic-drag model*). Numerical solutions for propagating cable waves are developed for the case of a long suspension subjected to a concentrated harmonic excitation source. Conclusions are subsequently drawn regarding the spatial decay of the resulting out-of-plane waves and the dynamic cable tension induced by these waves. The effect of these two nonlinear mechanisms is further explored through the analysis of two addition, linear models: (3) a simple linear taut string model without drag (the *simple model*); and (4) a linear taut string model with linear drag (the *linear drag model*). The simple model and the linear drag model are classical and are evaluated using closed-form techniques. In particular, the linear drag model is evaluated by first linearizing the hydrodynamic drag force model over one excitation period and then, via a Green's function formulation, evaluating forced wave propagation solutions. Results of both linear and nonlinear cable/fluid models are critically compared.

2. Nonlinear Cable/Fluid Models

Consider a uniform, flexible, cable submerged in a quiescent fluid as depicted in Figure 1. Following [2, 3], the cable is modeled as a one-dimensional elastic continuum with negligible bending and torsional stiffness, having density ρ_c, and supporting static tension $T_0(s)$. The

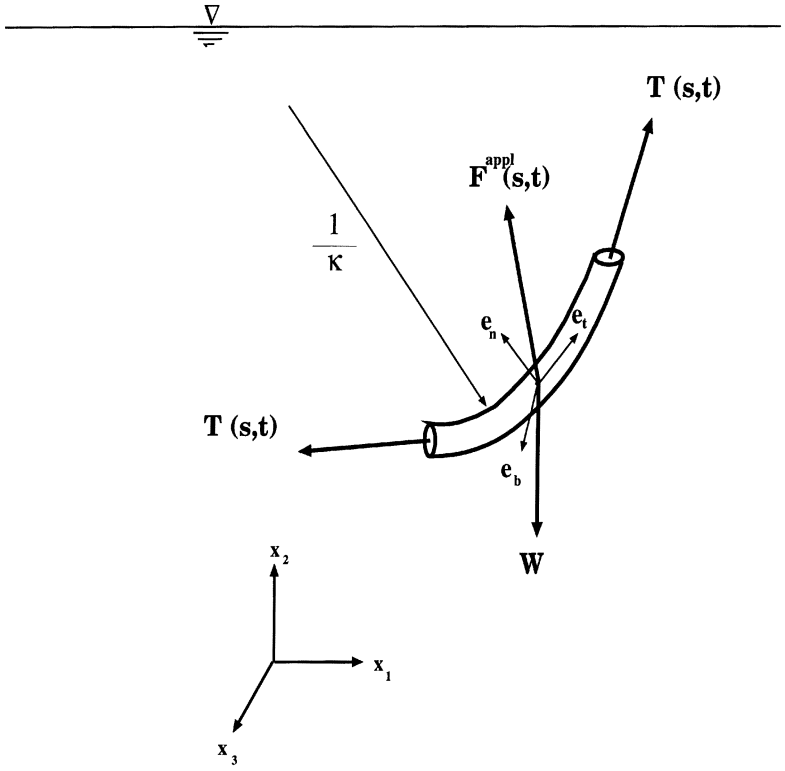

Figure 1. Free body diagram for an elastic submerged cable element. Three-dimensional displacement is referred to the equilibrium Frenet triad $\{\mathbf{e}_t, \mathbf{e}_n, \mathbf{e}_b\}$. T denotes the total tension in the cable, W is the weight per unit length, and κ is the centerline curvature.

spatial variable, s, is the arc length coordinate measured along the cable equilibrium centerline. Following a disturbance, the cable centerline may deform as described by the displacement $\mathbf{u}(s,t)$ shown in Figure 1. Here, we shall immediately focus attention on the bi-normal motion of the cable $u_3(s,t)$; that is, the motion component orthogonal to the plane formed by the cable equilibrium. While this motion component couples, in general, to components describing motion in the equilibrium plane [3], the present model will neglect this coupling. With this restriction, the resulting theory for out-of-plane dynamics reduces to that of a taut string and provides the opportunity to examine the relative importance of geometric and hydrodynamic nonlinearities in the context of the simplest (albeit approximate) cable theory. The conclusions drawn from this simple theory are subsequently extended to the geometrically more complex theory for in-plane response [1].

The equation governing the out-of-plane motion of a cable element Δs is

$$[F^{\text{hyd}} + F^{\text{elastic}} + F^{\text{appl}}]\Delta s = \rho_c A \Delta s u_{3,tt}, \tag{1}$$

where F^{elastic} represents the bi-normal component of the net elastic force/length, F^{hyd} represents the bi-normal component of the net hydrodynamic force/length, F^{appl} is any bi-normally applied external excitation/length. These force components are illustrated in Figure 1 which also illustrates the Frenet triad $(\mathbf{e}_t, \mathbf{e}_n, \mathbf{e}_b)$ used to define the bi-normal $(\mathbf{e}_b)$ direction. The equation of motion is augmented by the initial conditions

$$u_3(s, t=0) = u_{03}(s), \qquad u_{3,t}(s, t=0) = u_{03,t}(s), \tag{2}$$

where the functions $u_{03}(s)$ and $u_{03,t}(s)$ have finite norm on the infinite cable domain $-\infty < s < -\infty$. Moreover, the cable response satisfies classical radiation conditions for an infinite domain. The form of each force component in (1) is presently reviewed.

The net hydrodynamic force is composed of three major components, namely the Froude–Krylov forces F_{FK} deriving from wave pressure, hydrodynamic inertia forces F_m, and viscous drag forces F_D [23, 24]. Employing standard Morison assumptions leads to

$$F^{\text{hyd}} = F_{\text{FK}} + F_m + F_D, \tag{3}$$

$$F_{\text{FK}} = C_m \rho_w A \frac{\partial v_f}{\partial t}\,, \quad F_m = C_a \rho_w A \frac{\partial^2 u}{\partial t^2}\,, \quad F_D = C_D \frac{\rho_w d}{2}\,|v|v, \tag{4}$$

where v_f denotes the fluid particle velocity, v is the velocity of a cable material point relative to the fluid particle velocity, ρ_w is the density of water, and A is the cable cross sectional area of diameter d. The coefficients C_m, C_a, C_D, may be determined theoretically (in exceptional cases) or experimentally. For the quiescent fluid medium considered, herein the Froude–Krylov forces vanish and $v = \partial u/\partial t$. As a result, the net hydrodynamic force/length on a submerged cable in the bi-normal direction is

$$F^{\text{hyd}} = \left[\rho_w \frac{\pi d^2}{4}\,\frac{\partial^2 u_3}{\partial t^2} + C_D \frac{\rho_w d}{2}\,|u_{3,t}|u_{3,t}\right], \tag{5}$$

where $C_a = 1$ and the drag coefficient, C_D, is chosen from experimental data [23]. Further consideration of a relative fluid velocity field leads to convective nonlinearities that can be accounted for using established extensions as in [22].

Stretching of the cable centerline induces the total cable tension T. The static tension component T_0 represents the dominant stiffness mechanism for the long cable suspensions of interest in this study (negligible bending, shear, and torsional stiffnesses). The net elastic force/length in the bi-normal direction acting on the element is

$$F^{\text{elastic}} = \frac{\partial(T\phi)}{\partial s} = \phi \frac{\partial T}{\partial s} + T \frac{\partial \phi}{\partial s}\,, \tag{6}$$

where $\phi = \partial u_3/\partial s$ and

$$T(s,t) = EA(\varepsilon_0 + \varepsilon_d), \tag{7}$$

$$\varepsilon_0 = \frac{T_0}{EA}\,, \qquad \varepsilon_d = \frac{1}{2}\,(u_{3,s})^2. \tag{8}$$

Here ε_0 denotes the static strain and ε_d is the dynamic (Lagrangian) strain. The resultant Young's modulus for the cable material is E. Finally, the applied force/length, F^{appl}, represents any prescribed excitation/length in the bi-normal direction. The central, concentrated harmonic excitation source, $F^{\text{appl}} = F_0 \delta(s) e^{j\omega t}$, is selected for all the examples in this study as the means to examine wave propagation characteristics.

3. Four Model Formulations

To achieve the objective of this investigation, four different models for the bi-normal motion of a taut elastic cable are evaluated. Two of these models are linearizations of Equation (1);

one without and one with hydrodynamic drag (dissipation). Specifically, the two linear models are: (1) a simple linear taut string model without drag (the *simple model*); and (2) a simple linear taut string model with an equivalent linearized hydrodynamic drag term (the *linear drag model*). The linear models are both evaluated analytically. The nonlinear effects are captured in two nonlinear models, beginning with: (3) a simple linear string with the full nonlinear hydrodynamic term (the *nonlinear drag model*); and (4) a nonlinear elastic string model with the full nonlinear hydrodynamic drag term (the *nonlinear elastic-drag model*). The nonlinear models are evaluated using numerical methods.

3.1. LINEARIZED MODELS

3.1.1. *Simple Model*

Neglecting the hydrodynamic forces in (1) and linearizing (1) leads to the nonhomogeneous linear, one-dimensional wave equation (Cauchy problem [8]) defining the simple model:

$$c_t^2 u_{3,ss} + \frac{1}{\rho_c A} F^{\text{appl}} = u_{3,tt}, \tag{9}$$

where $c_t = \sqrt{T_0/\rho_c}$ is the phase velocity and T_0 is equilibrium cable tension. Here, attention will focus on the steady state response to the applied harmonic excitation source introduced in Section 2.

The solution for forced wave propagation is readily available in the literature; see, for instance [8]. The concentrated harmonic forces induces the rightward propagating wave

$$u_3(s,t) = -\frac{jF_0}{2\rho A c_t \omega} \exp\{j(\gamma_0 s - \omega t)\} + \text{C.C.} \quad \text{on} \quad 0 < s < \infty, \tag{10}$$

in which $F_0(\omega)$ is the amplitude (frequency) of the harmonic excitation and $\gamma_0 = \omega/c_t$ is the wave number. Here, C.C. represents the complex conjugate of the preceding terms. The concentrated source also induces leftward propagation waves, the form of which is obvious from (10).

3.1.2. *Linear Drag Model*

The simple model above is an extreme idealization for a submerged cable and is included here for direct comparison with models of greater fidelity. A simple model with greater fidelity follows from linearization of the equation of motion (1). To this end, the linearized equation of motion can be decomposed as

$$F_L^{\text{elastic}} + F_{DL}^{\text{hyd}} + F_m^{\text{hyd}} + F^{\text{appl}} = \rho_c A u_{3,tt}, \tag{11}$$

where F_L^{elastic} denotes the linear elastic force component, F_{DL}^{hyd} and F_m^{hyd} denote the hydrodynamic forces composed of a linearized drag component and an added mass component, and F^{appl} denotes the external excitation. The force components are

$$F_L^{\text{elastic}} = [T_0 u_{3,s}]_{,s}, \qquad F^{\text{appl}} = F\delta(s)\exp(j\omega t), \tag{12}$$

$$F_L^{\text{hyd}} = -F_{DL}^{\text{hyd}} - F_m^{\text{hyd}} = -\frac{1}{2} C_{DL}\rho_w d u_{3,t} - \rho_w A u_{3,tt}, \tag{13}$$

where C_{DL} is the equivalent linear drag coefficient.

To obtain C_{DL}, the linearized hydrodynamic drag force is selected to minimize the squared error between the linear drag model and the (quadratic) Morison's drag model over one period of motion. Thus, C_{DL} is chosen such that

$$\int_0^{T_p} (F_{D_L}^{\text{hyd}} - F_{D_{NL}}^{\text{hyd}})^2 \, \mathrm{d}t \tag{14}$$

is minimized [23], where

$$F_{D_L}^{\text{hyd}} = \frac{1}{2}\,\rho_2 d C_{DL} u_{3,t}, \qquad F_{D_{NL}}^{\text{hyd}} = \frac{1}{2}\,\rho_w d C_D u_{3,t}|u_{3,t}|. \tag{15}$$

After some manipulation, the equivalent linear drag coefficient is found to be

$$C_{DL} = \frac{8}{3\pi}\, C_D \omega \bar{u}_3, \tag{16}$$

where ω and $\bar{u}_3$ denote the frequency and amplitude of the cable motion.

Substituting Equations (12) and (13) into (11) leads to the nonhomogeneous and dissipative linear wave equation defining the linear drag model:

$$c_t^2 u_{3,ss} - \left(\frac{\rho_w d}{2\rho_c A}\, C_{DL}\right) u_{3,t} + \left(\frac{1}{\rho_c A}\right) F_0 \delta(s) e^{j\omega t} = \left(\frac{\rho_c + \rho_w}{\rho_c}\right) u_{3,tt}. \tag{17}$$

The forced wave propagation response can be determined in closed form by the Green's function approach developed in [2]. In particular, the concentrated harmonic force considered herein induces the rightward propagating wave

$$u_3(s,t) = \frac{jF_0}{2\rho_c A c_t^2 \gamma_d} \exp\{-s\gamma_I\} \exp\{s\gamma_R - \omega t\} + \text{C.C.} \quad \text{on} \quad 0 < s < \infty, \tag{18}$$

where γ_R and γ_I are the real and imaginary parts of the wave number, γ_d as given by

$$\gamma_d^2 = \frac{\beta}{c_t^2}\,\omega^2 + j\frac{\Psi_L}{c_t^2}\,\omega, \tag{19}$$

$$\gamma_R = \pm\left\{\frac{\alpha_1}{2} + \sqrt{\frac{\alpha_1^2}{4} + \alpha_2^2}\right\}^{1/2}, \quad \gamma_I = \pm\left\{-\frac{\alpha_1}{2} + \sqrt{\frac{\alpha_1^2}{4} + \alpha_2^2}\right\}^{1/2}, \tag{20}$$

$$\alpha_1 = \frac{\beta}{c_t^2}\,\omega^2 \quad \text{and} \quad \alpha_2 = \frac{\Psi_L}{c_t^2}\,\omega. \tag{21}$$

Here $\Psi_L = (\rho_w d/2\rho_c A) C_{DL}$ and $\beta = (\rho_c + \rho_w)/\rho_c$. Thus, the cable response is determined once the drag coefficient C_{DL} is determined. In view of the fact that C_{DL} depends on the amplitude of the response (16), the solution must be found iteratively as follows. First, an initial guess of the amplitude $\bar{u}_3$ is used to compute the draf coefficient (16) which is then used to compute the response through (18). The computed new response amplitude $\bar{u}_3$ is then used to adjust C_{DL} and the procedure is repeated until convergence is achieved for $\bar{u}_3$.

3.2. NONLINEAR MODELS

3.2.1. *Nonlinear Drag Model*

The nonlinear drag model results from considering the hydrodynamic drag as the sole nonlinear mechanism. In this case, the complete nonlinear Morison Equation (5) is utilized together with the linearized elastic force component of (12). Substituting these equations in (1) leads to the nonlinear drag model

$$c_t^2 u_{3,ss} - \Psi u_{3,t}|u_{3,t}| + \Upsilon F^{\text{appl}} = \beta u_{3,tt}, \tag{22}$$

where

$$\Psi = \frac{\rho_w d}{2\rho_c A}\, C_D, \quad \Upsilon = \frac{1}{\rho_c A}\,, \quad \beta = \frac{\rho_c + \rho_w}{\rho_c}\,. \tag{23}$$

The nonlinear drag model, which is quadratic in the cable velocity, is evaluated using the numerical procedure described in Section 4.

3.2.2. *Nonlinear Elastic-Drag Model*

The nonlinear elastic-drag model results from simultaneous consideration of the nonlinearities due to hydrodynamic drag and finite cable stretching. In this case, the linear and nonlinear elastic forces are

$$F_L^{\text{elastic}} + F_{NL}^{\text{elastic}} = \left[\left(T_0 + \frac{1}{2}\, EA u_{3,s}^2\right) u_{3,s}\right]_{,s} \tag{24}$$

which capture the finite stretching of the string centerline [20]. Substituting (23) and (5) in the equation of motion (1) yields the nonlinear elastic-drag model

$$c_t^2 u_{3,ss} - \Psi u_{3,t}|u_{3,t}| + \frac{1}{2}\, c_l^2 [u_{3,s}^3]_{,s} + \Upsilon F^{\text{appl}} = \beta u_{3,tt}, \tag{25}$$

where c_l is the classical longitudinal wave speed of a rod, $c_l = \sqrt{E/\rho_c}$.

4. Numerical Solution Model

Numerical solutions are pursued herein using a space-time finite difference algorithm. Consider a cable of length L described by N internal nodes. Let u_j^i denote the bi-normal displacement of the cable at node j and at time step i. Fourth-order central differencing in space is employed for first and second spatial derivatives. Second-order backwards differencing in time is employed for formulating first and second order time derivatives [25]. This discretization forms a time-marching algorithm for solution of the nodal displacements u_j^i and velocity v_j^i as given by

$$u_j^{i+1} = u_j^i + v_j^i \Delta t + \frac{1}{2}\, \beta_1 \Delta t^2 (a_j^i + \beta_2 a_j^{i+1}), \tag{26}$$

$$v_j^{i+1} = v_j^i + \frac{1}{2}\, \alpha_1 \Delta t (a_j^i + \alpha_2 a_j^{i+1}). \tag{27}$$

Here, Δt is the time step and β_1, β_2, α_1 and α_2 are integration parameters which are selected as 0.5, 1.0, 0.5, and 1.0, respectively.

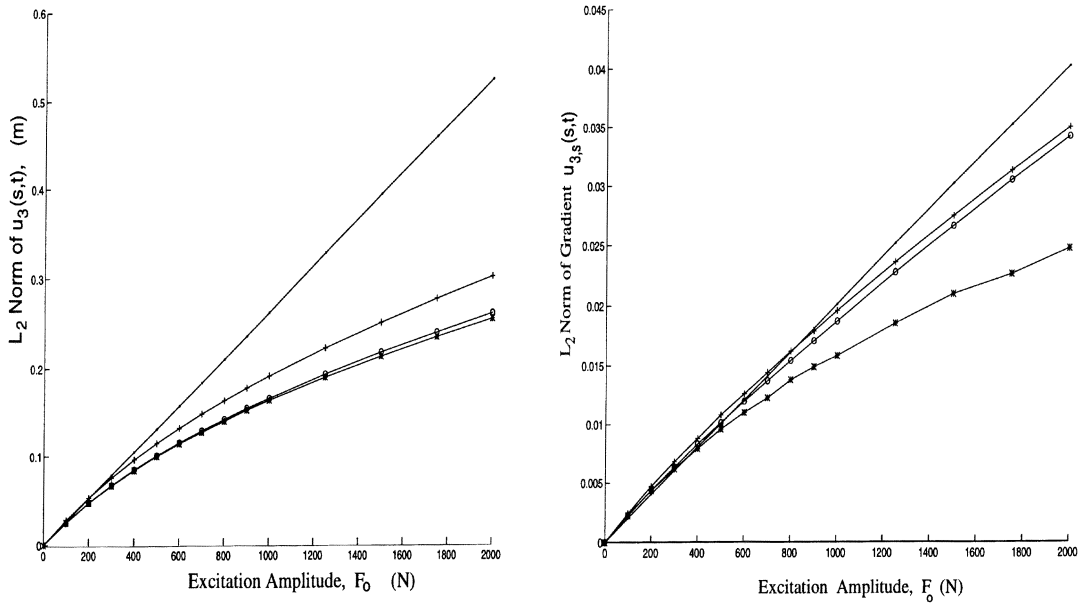

(A) (B)

Figure 2. L_2 norm of (A) the displacement and (B) the displacement gradient along the first ten meters from the source. Norm is computed using numerical solutions to all four models for the example cable suspension defined in Table 1. The excitation frequency is $\omega = 10$ rad/s. Simple model $\cdots$; linear drag model ++++; nonlinear drag model $\circ\circ\circ\circ$; nonlinear elastic-drag model $****$.

The nodal acceleration a_j^{i+1} are collected as the vector $\mathbf{A}^{i+1}$ and evaluated from the approximate equation of motion:

$$\mathbf{M}\mathbf{A}^{i+1} + \mathbf{C}|\mathbf{V}^i|\mathbf{V}^i + \mathbf{K}\mathbf{U}^i = (\mathbf{F}^{\text{appl}})^i, \tag{28}$$

where $\mathbf{U}^i$ and $\mathbf{V}^i$ are vectors containing the nodal displacements and velocities, respectively, and $(\mathbf{F}^{\text{appl}})^i$ is the prescribed excitation (vector). The **M** and **C** matrices are constants, but **K** is a function of the nodal displacements due to the geometric nonlinearity. This algorithm is a two-step, three-value method.

5. Results and Discussion

In all examples to follow, consider the response of an infinite cable subject to a concentrated harmonic excitation source in the out-of-plane direction at the origin ($s = 0$). Let F_0 and ω denote the amplitude and frequency of the source

$$F^{\text{appl}} = F_0\delta(s)e^{j\omega t}. \tag{29}$$

As a first example, consider a cable suspension with properties defined in Table 1. This suspension is subjected to a concentrated harmonic source which, in the present example, has frequency $\omega = 10$ rad/s. Figure 2 provides a direct comparison of the results computed from all four models. Shown in Figure 2A (2B) is the L_2 norm of the computed cable displacement (displacement gradient) for each model. The L_2 norm, which is computed over

Table 1. Cable parameter values for a representative steel wire rope suspension [12].

Sample submerged steel wire rope		
Cable property	Symbol	Values
Young's modulus	E	1.0×10^{11} Pa
Density	ρ_c	3750 kg/m^3
Cross sectional area	A	314.2 mm^2
Static tension	T_0	21.2 kN
Length	L	2000 m
Phase speed	c_t	134 m/s

$0 \leq s \leq 10$ m, is shown as a function of the excitation amplitude F_0 (N). For the simple model, these norms increase linearly with F_0 as required by linearity. Focusing first on the displacement norm of Figure 2A, note that all models predict nearly identical norms for excitation amplitudes below 100 N. For excitation amplitudes exceeding 100 N, however, the three models with dissipation (linear drag, nonlinear drag, and nonlinear elastic-drag) predict response amplitudes significantly less than the simple model. The displacement norm computed from the nonlinear drag and nonlinear elastic-drag models are nearly identical and both substantially less than that of the linear drag model.

Figure 2B illustrates similar results for the norm of the gradient of the displacement $(u_{3,s})$. This gradient is an important quantity that is subsequently used to compute the dynamic tension as described in the following. Inspection of Figure 2B reveals that the simple model first under predicts the gradient for excitation amplitudes less than 400 N when compared to the three models with dissipation. For excitation amplitude in excess of 400 N, however, the simple model leads to large overpredictions. For all excitation amplitudes, the norm of the gradient of the linear drag model is comparable to that of the nonlinear drag model, but both exceed that of the nonlinear elastic-drag model.

The previous solutions for the displacement field can be used to compute the dynamic cable tension which is an important metric of cable response in applications (e.g., dynamic tension influences cable survivability and the positioning and response of attached bodies). The dynamic tension is evaluated using

$$T_d(s,t) = EA\varepsilon_d, \tag{30}$$

where ε_d (8) is the Lagrangian strain of the centerline.

The L_2 norm of the dynamic tension for all four models is illustrated in Figure 3 for comparison. The results follow directly from those of Figure 2B. Note that for the simple model, the dynamic tension, which can be calculated in a closed form, grows exactly quadratically with excitation amplitude. Moreover, in the region of large excitation amplitude, this model greatly overestimates the dynamic tension. This error limits the utility of this model for design. Again note the close agreement of the linear and nonlinear drag models which also overpredict the dynamic tension relative to the nonlinear elastic-drag model. Thus, the importance of the nonlinear geometric stiffening increases with increasing excitation amplitude.

The effect of nonlinear geometric stiffening is further examined in Figure 4 which compares the cable response for the nonlinear drag model, and the nonlinear elastic-drag model. The displacement profiles are illustrated at one representative time. Observe that the wavelength

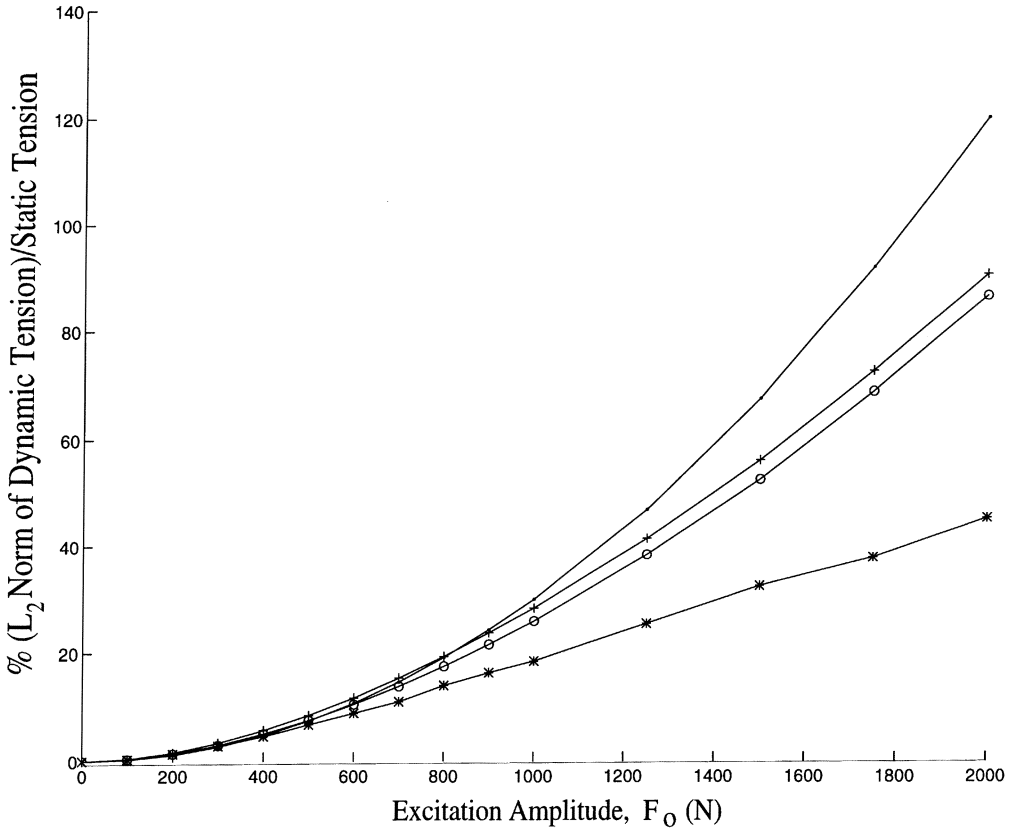

Figure 3. L_2 norm of dynamic tensionof the cable along the first ten meters from the source. This tension norm is presented as a percentage of the static tension and is computed for all four models for the example cable suspension defined in Table 1. The excitation frequency is $\omega = 10$ rad/s. Simple model $\cdots$; linear drag model ++++; nonlinear drag model $\circ\circ\circ\circ$; nonlinear elastic-drag model $****$.

of the disturbance increases slightly as a result of the additional nonlinear geometric stiffness. Similarly this geometric stiffening reduces the gradient of the wave form and leads to a marked reduction in displacement in the vicinity of the concentrated load.

The spatial distribution of the dynamic cable tension is illustrated in the results of Figure 5 computed using the nonlinear elastic-drag model for the case $\omega = 10$ rad/s and $F_0 = 800$ N. The dynamic tension wave profile is illustrated in Figure 5A with the associated power spectral density (*versus* wave number) in Figure 5B. Inspection of these results reveals two major points. First, application of an external excitation in the bi-normal direction creates a significant tension wave that propagates outwards from the source (note dynamic tension is reported as a percentage of static tension). Second, the tension waves along the submerged cable sharply decrease as they propagate away from the source. This reduction of dynamic tension derives from the dissipation of energy by hydrodynamic drag. From Figure 5B, note that the wave numbers less than $\gamma = 0.25$ (m^{-1}) have significant effect on the tension wave. In particular, two special wave numbers, one close to zero and another close to $\gamma = 0.16$ have pronounced influence. The dominant role of these wave numbers is further explained using the results of Figure 6.

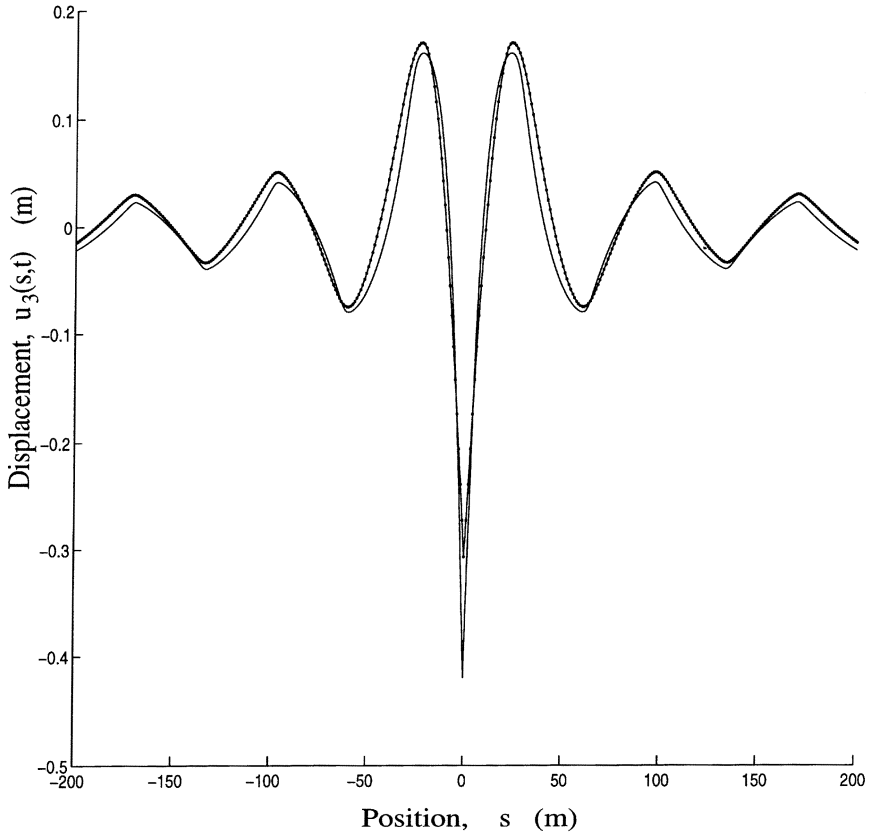

Figure 4. Comparison of the displacement predicted by the nonlinear drag and the nonlinear elastic-drag models. Displacement profiles illustrated at time $t = 7.9$ sec for excitation characterized by $F_0 = 3$ kN and $\omega = 10$ rad/s. The cable material and geometric properties are listed in Table 1. Nonlinear drag model —-; nonlinear elastic-drag model · · · ·.

The results of Figure 6 illustrate wave propagation characteristics for three cable models; namely the simple model (A1, A2), the nonlinear drag model (B1, B2), and the nonlinear elastic-drag model (C1, C2). Results in the first column illustrate the wave profile at the representative time $t = 5.8$ sec which corresponds to approximately three excitation cycles ($\omega = 10$ rad/s). Results in the second column illustrate the corresponding power spectral densities. For the simple model (A1), the waves propagate uniformly without attenuation from the source as expected. In contrast, for the nonlinear drag (B1) and nonlinear elastic-drag models (C1), the wave amplitudes sharply attenuate with distance from the source due to fluid damping.

The power spectral densities provide further distinction between these models. For the simple model (A2), the power spectral density essentially vanishes for all wave numbers except that corresponding to excitation frequency ($\omega = 10$ rad/s) for the phase velocity ($c_t = 152$ m/s); namely $\gamma = \omega/c_t = 0.066\,\mathrm{m}^{-1}$. By contrast, the power spectral densities for the two nonlinear models illustrate measurable contributions for all wave numbers $\gamma \leq 0.15$ (m^{-1}) with maximum contribution in the neighborhood of $\gamma = 0.08$ (m^{-1}). Comparison of (B2) and (C2) reveals a small discernible difference between the two nonlinear models. Note that the power spectral density for the nonlinear elastic-drag model (C2) is greater (lesser) than that of

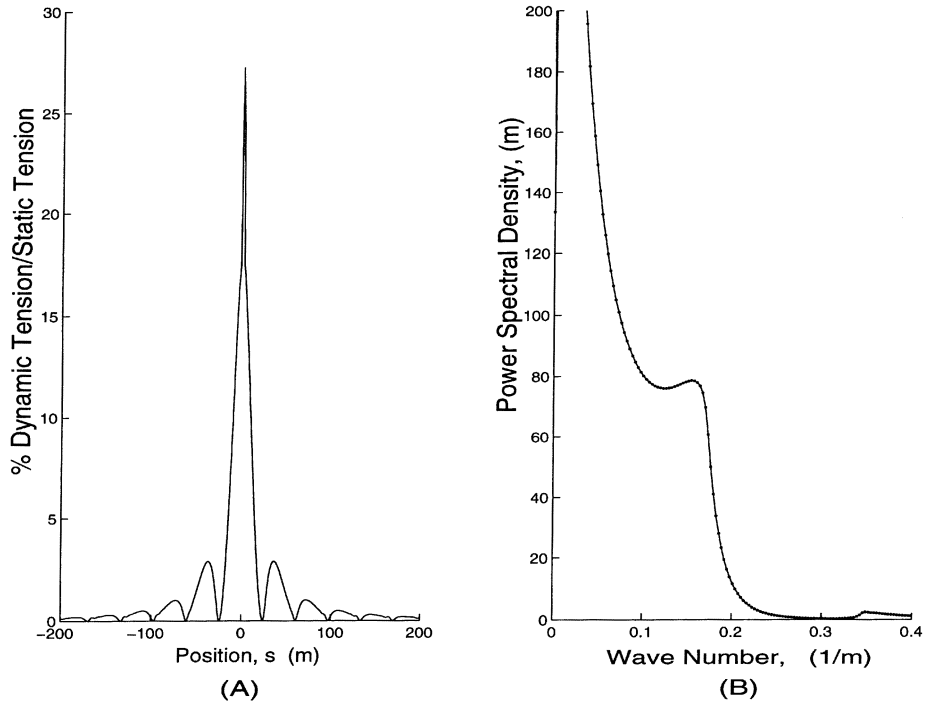

Figure 5. (A) Dynamic tension profile induced by a concentrated harmonic source of magnitude of $F_0 = 800$ N and frequency $\omega = 10$ rad/s. (B) The associated power spectrum. The cable material and geometric properties are listed in Table 1.

the nonlinear drag model (B2) for the wave numbers $\gamma \leq 0.08$ ($\gamma \geq 0.08$). Thus, waves for the nonlinear elastic-drag model will propagate faster than those for the nonlinear drag model due to the increased (nonlinear) stiffness. Note also that, at this excitation frequency, disturbances propagate visibly slower for both nonlinear models in comparison with the simple model as can be observed from the results in either column.

The results of Figure 6B1 and 6C1 illustrate considerable spatial decay due to hydrodynamic drag. This effect is further examined through Figure 7 which illustrates the envelope (loci of response maxima) of the cable displacement along the suspension computed using the nonlinear elastic-drag model. The three envelopes shown correspond to three values of the excitation frequency ($\omega = 2$, 3, 10 rad/s). Note that the spatial decay rate is greatest near the source and that this decay rate increases with excitation frequency in direct response to higher hydrodynamic drag. Moreover, the amplitude of the response decreases with increasing excitation frequency as expected.

6. Conclusion

This investigation focuses on two nonlinear mechanisms governing the propagation of out-of-plane structural waves along elastic cables in a fluid medium. The nonlinear mechanisms model (1) hydrodynamic drag, and (2) finite centerline stretching (geometric stiffening). The influence of these nonlinear mechanisms is highlighted by examining computed response solution to four models. Examples focus on cable response to a concentrated harmonic source.

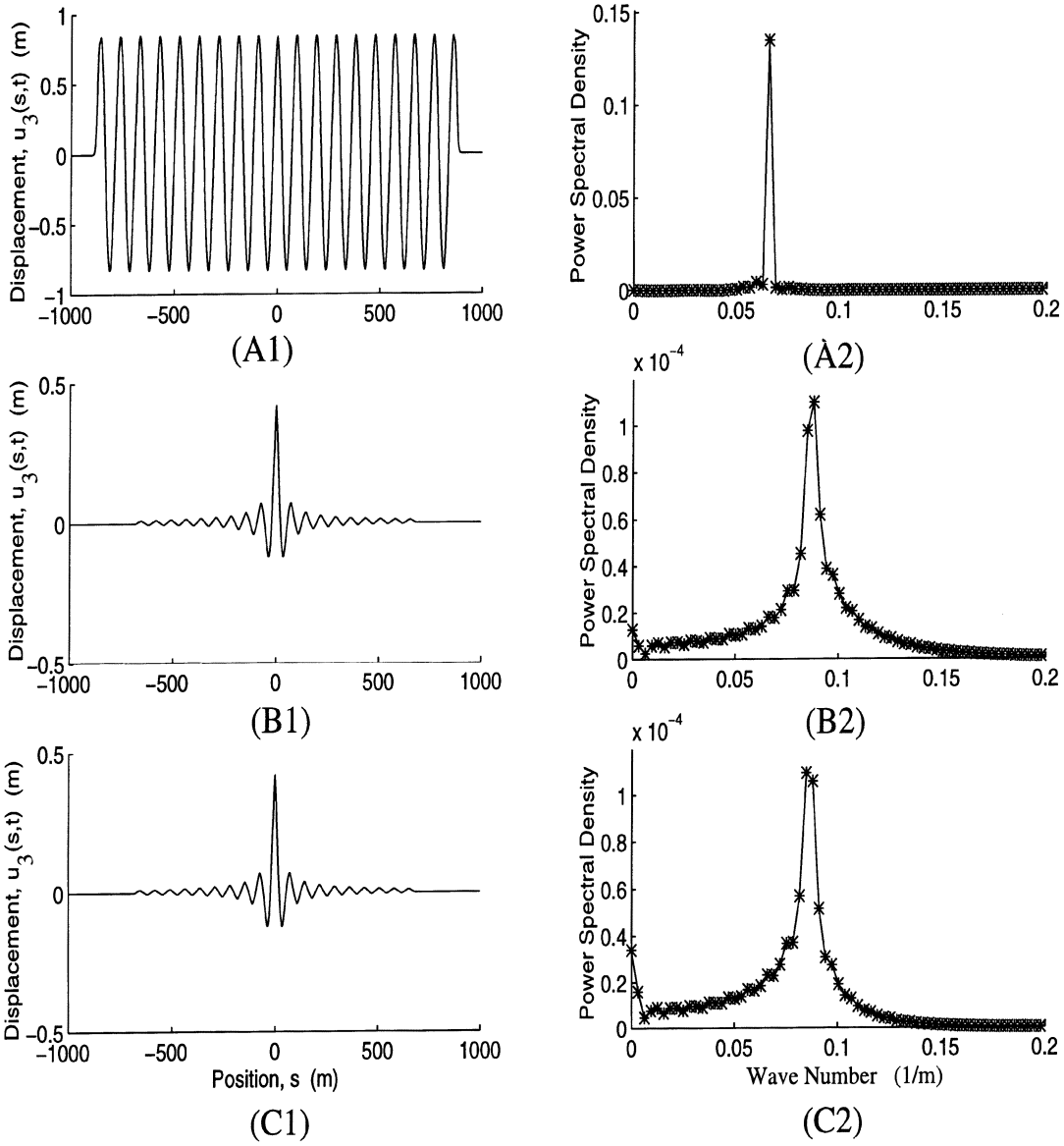

Figure 6. Response to a harmonic source characterized by $F_0 = 3$ kN and $\omega = 10$ rad/s at the representation time $t = 5.8$ sec. Response and associated power spectra for the simple model (A1, A2), the nonlinear drag model (B1, B2), and nonlinear elastic-drag model (C1, C2). The cable material and geometric properties are listed in Table 1.

The major effect of hydrodynamic drag is to attenuate cable response away from the source and to do so sharply as the excitation frequency increases. The major effect of geometric stiffening is to increase the wave propagation speed (rendering the model dispersive). Solutions for the cable response were subsequently used to estimate dynamic cable tension for all four models. Comparison of the L_2 norm of the dynamic tension reveals that the simple model greatly overestimates the dynamic tension rendering this model inadequate for design calculations. By contrast, the linearized drag model provides a rather good prediction when compared to both nonlinear models (the nonlinear drag model and the nonlinear elastic-drag models) for the

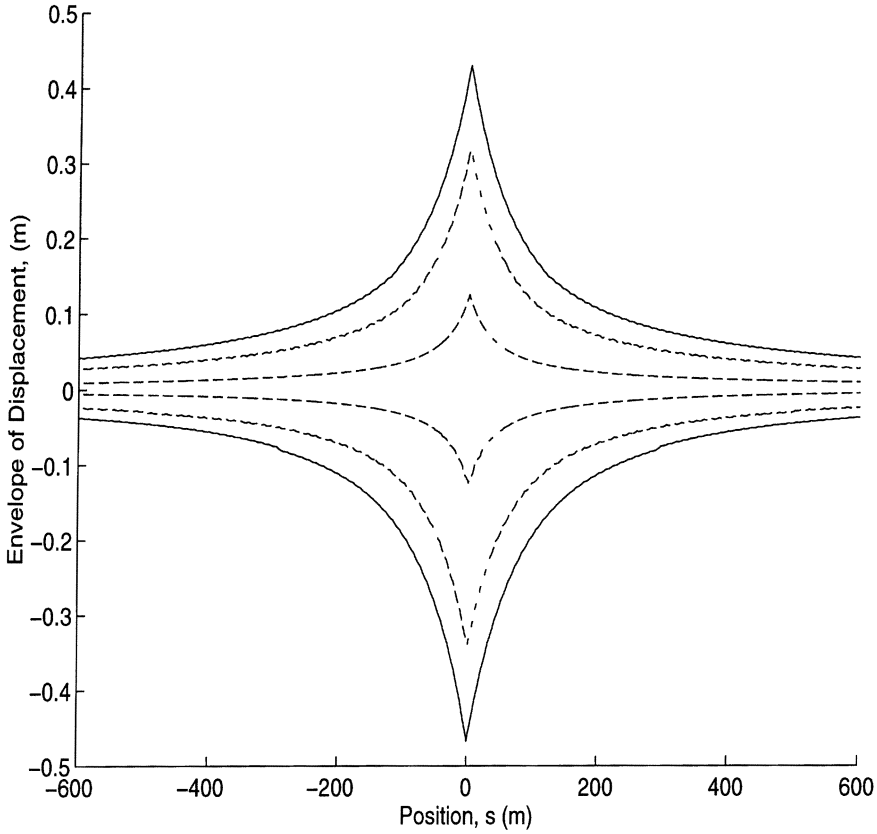

Figure 7. The displacement envelope of the cable response for three values of the external excitation frequency as predicted by the nonlinear elastic-drag model. The excitation is characterized by $F_0 = 2$ kN and frequencies $\omega = 2$ rad/s —, $\omega = 3$ rad/s – – –, $\omega = 10$ rad/s · – · – ·. The cable material and geometric properties are listed in Table 1.

small to moderate excitation levels considered herein. Thus, the linearized drag approximation appears to be an acceptable and reliable approximation for design calculation. For the largest excitation levels considered herein, the tension computed by the nonlinear elastic-drag model forms a lower bound to the tension computed using all other models due to the added stiffness generated by finite centerline stretching.

Acknowledgement

The authors gratefully acknowledge the support of the Office of Naval Research through grant no. N00014-89-J-3159.

References

1. Behbahani-Nejad, M., 'Linear and nonlinear wave propagation characteristics of elastic cables with and without fluid interaction', PhD Thesis, The University of Michigan, Ann Arbor, MI, 1997.
2. Behbahani-Nejad, M. and Perkins, N. C., 'Forced wave propagation in elastic cables with small curvature', in *15th Biennial ASME Conference on Mechanical Vibration and Noise*, Boston, MA, September 1995, Vol. 3, pp. 1457–1464.

3. Perkins, N. C. and Mote, C. D., 'Three-dimensional vibration of travelling elastic cable dynamics', *Journal of Sound and Vibration* **114**(2), 1987, 325–340.
4. Behbahani-Nejad, M. and Perkins, N. C., 'Motion and tension waves in elastic cables', in *Proceedings International Symposium on Cable Dynamics*, Liège, Belgium, October 1995, Vol. 1, pp. 37–44.
5. Den Hartog, J. P., *Mechanical Vibrations*, McGraw-Hill, New York, 1955.
6. Graff, K. F., *Wave Motion in Elastic Solids*, Ohio State University Press, Columbus, OH, 1975.
7. Meirovitch, L., *Analytical Methods in Vibrations*, MacMillan, New York, 1967.
8. Hildebrand, F. B., *Advanced Calculus for Engineers*, Prentice-Hall, Englewood Cliffs, NJ, 1960.
9. Achenbach, J. D., *Wave Propagation in Elastic Solids*, Elsevier, New York, 1984.
10. Irivine, H. M., *Cable Structures*, MIT Press, Cambridge, MA, 1981.
11. Li, L. and Vandiver, J. K., 'Wave propagation in strings with rigid lumps', *ASME Journal of Vibration and Acoustics* **117**(4), 1995, 493–500.
12. Grosenbaugh, M. A., 'The effect of hydrodynamic damping on the tension of oceanographic surface moorings', in *Proceedings International Symposium on Cable Dynamics*, Liège, Belgium, October 1995, Vol. 1, pp. 85–92.
13. Chapman, D. A., 'Effects of ship motion on a neutrally-stable towed fish', *Ocean Engineering* **9**(3), 1982, 189–220.
14. Dowling, A. P., 'The dynamics of towed flexible cylinders. Part II. Neutrally buoyant elements', *Journal of Fluid Mechanics* **187**, 1988, 533–571.
15. Hudson, G. E., 'Dispersion of elastic waves in solid circular cylinders', *Physical Review* **63**, 1943, 46–51.
16. Mindlin, R. D. and Herrmann, G., 'A one-dimensional theory of compressional waves in an elastic rod', in *Proceedings First U.S. National Congress of Applied Mechanics*, 1952, pp. 187–191.
17. Morley, L. S., 'Elastic waves in a naturally curved rod', *Journal of Mechanics and Applied Mathematics* **XIV**(2), 1961, 155–172.
18. Mead, D. J., 'Wave propagation and natural modes in periodic systems: I. Mono-coupled', *Journal of Sound and Vibration* **40**(1), 1975, 1–18.
19. Doyle, J. F., *Wave Propagation in Structures*, Springer-Verlag, New York, 1989.
20. Malvern, L. E., *Introduction to the Mechanics of a Continuous Medium*, Prentice Hall, Englewood Cliffs, NJ, 1969.
21. McGhie, R. D., 'Flexural wave motion in infinite beam', *Journal of Engineering Mechanics* **116**(3), 1990, 531–547.
22. Newman, J. N., *Marine Hydrodynamics*, MIT Press, Cambridge, MA, 1977.
23. Chakrabarti, S. K., *Hydrodynamics of Offshore Structures*, Springer-Verlag, New York, 1987.
24. Patel, Minoo H., *Dynamics of Offshore Structures*, Butterworths, Boston (London), 1989.
25. Schiesser, W. E., *The Numerical Method of Lines*, Academic Press, San Diego, CA, 1991.